BACHELOR

Seebeck coefficient and controlled doping measurements on semiconducting polymers

van Dijk, W.

Award date:
2014

Seebeck coefficient and controlled doping measurements on semiconducting polymers

By Wessel van Dijk

Bachelor thesis
Eindhoven University of Technology
Applied Physics
Molecular Materials and Nanosystems

Supervisors
prof. dr. ir. Martijn Kemerink
ir. Stephan van Reenen

Abstract

In this report experiments are described to measure the Seebeck coefficient of a semiconducting polymer. These experimens have been performed on PEDOT:PSS PH1000 yielding Seebeck coefficients in the range of $S = 10^{-5}$ V/K.

Using organic electrochemically gated transistor devices, the effects of doping on the electrical properties of several organic semiconductors have been studied. In summary, we have measured the doping density, conductivity and mobility of these devices, containing the organic semiconductors Super-Yellow PPV and F8BT. The solvent used for the electrolyte has been altered between two measurement series, resulting in the uncertainty in doping density measurements decreasing by a factor ten in some cases. Because of this increase of quality of our measurements we were able to determine the direct effect of controlled doping on the mobility and conductivity of an F8BT sample.

Table of contents

ABSTRACT 2

TABLE OF CONTENTS 3

INTRODUCTION 4

2 THEORY 2.1 ORGANIC SEMICONDUCTORS 5

2.2 SEEBECK-PELTIER EFFECT 6
2.3 ELECTRICAL CONDUCTIVITY 7
2.4 DERIVATION OF THE THERMO ELECTRICAL FIGURE OF MERIT 8
2.5 ORGANIC ELECTROCHEMICALLY GATED TRANSISTORS 11

3 EXPERIMENTAL SETUP 12

3.1 SEEBECK MEASUREMENTS 12
3.2 SAMPLES 14

4 PRELIMINARY EXPERIMENTS 15

4.1 SEEBECK EXPERIMENT 15
4.2 PRELIMINARY DOPING EXPERIMENTS 19

5 RESULTS AND DISCUSSION 22

5.1 SUPER-YELLOW PPV SERIES 22
5.2 F8BT – FIRST SERIES 24
5.3 F8BT – SECOND SERIES 28

6 CONCLUSION 32

7 OUTLOOK 33

10 SOURCES 34

Introduction

Organic solar cells could be a low cost solution to the energy problem in the world. The main disadvantages associated with organic photovoltaic cells are low efficiency, low stability and low strength compared to inorganic photovoltaic cells.

One way of increasing the efficiency of these plastic solar cells would be to make them not only use the energy of the visible light of the sun. The research described in this report is aimed at the conversion of energy from the infrared part of the sunlight to electrical energy. These so called thermoelectric generators (TEGs) convert heat into electrical energy.

The figure of merit *ZT* indicates the potential applicability of a material for the use in a TEG. This figure of merit is determined by the electrical conductivity, the thermal conductivity and the Seebeck coefficient. The Seebeck coefficient is defined as the thermo voltage that arises when a temperature difference of one Kelvin is applied over a material.

In this report several experiments are described to measure the Seebeck coefficient of PEDOT:PSS PH1000, a semiconducting polymer. These experiments have been performed, yielding Seebeck coefficients in the range of $S = 10^{-5}$ V/K.

The aim of the experiments described in this report is to optimize the so called power factor $S^2\sigma$, which is part of ZT, using controlled doping. By using organic electrochemically gated transistors on organic semiconductors called PPV and F8BT, the effects of doping on the electrical properties of the organic semiconductors are studied. However, the effect of doping the active material on the Seebeck coefficient is left open for future research.

2 Theory

2.1 Organic semiconductors

Generally speaking, synthetic polymers are used as electrically insulating material. There is however a class of synthetic polymers, called intrinsically conductive polymers (or ICP‘s), which has electrical, magnetic and optical properties typical of metals and semiconductors[1]. The configuration of these polymers causes the formation of high-energy orbitals in which electrons are relatively loosely bonded to their atoms. Because of these loosely bonded electrons, application of an electric or magnetic field can induce charge movement within the material. PEDOT:PSS is an example of these kinds of polymers, its carbon atoms have altering single and double bonds, resulting in the described high-energy orbitals.

The insulating, semiconducting or conducting characteristics of a material are determined by the band gap. The band gap is the distance in energy between valence band, the highest occupied molecular orbital (or HOMO), and the conducting band, the lowest unoccupied molecular orbital (LUMO). The LUMO energy level can attract electrons and has a higher energy than the HOMO energy level, which can give up electrons. The conducting mechanism is generated by the carrier movement through the LUMO by (negatively charged) electrons and through the HOMO by the (positively charged) holes.
In this band structure picture, the Fermi Level can be considered to be a hypothetical energy level of an electron, such that this energy level would have a 50% probability of being occupied at any given time. The Fermi level does not necessarily correspond to an actual energy level (in an insulator the Fermi level lies in the band gap), nor does it require the existence of a band structure. In an intrinsic or lightly doped semiconductor, the Fermi level lies in the band gap between the HOMO and the LUMO, where there are no available states.

An organic semiconductor is now an organic material which has electrical conductivity between that of a conductor and that of an insulator. In these semiconductors, electrical conductivity arises due to the presence of electrons in a state near the Fermi level. One important feature of semiconductors is that their conductivity can be controlled by doping with impurities and gating with electric fields. Doping and gating move the Fermi level E_F closer to the edge of the conduction or valence band, greatly increasing the number of partially filled states. This enhances carrier transport through these bands.

2.2 Seebeck-Peltier effect

When a temperature difference ΔT is applied over a semiconducting material, a thermo voltage is created which scales with the temperature difference, this is called the Seebeck effect [3]. Its counterpart, the Peltier effect, is the effect that a voltage difference applied over a material induces an electronic current that carries a heat flow through the material. Both effects are schematically shown in the following figure.

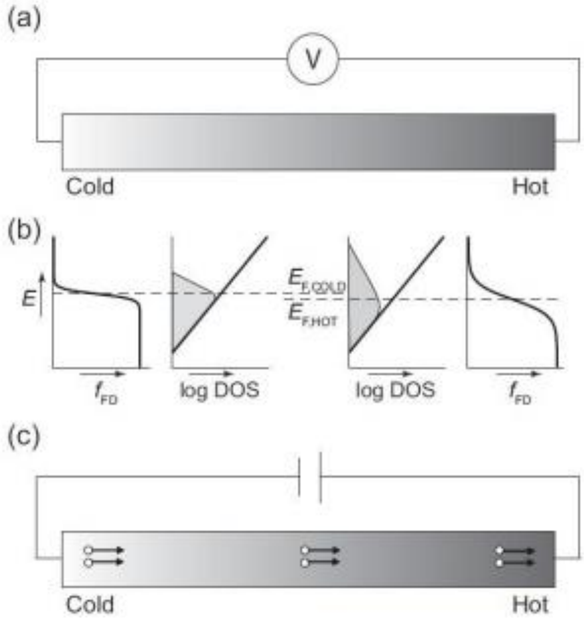

Figure 1 A schematical representation of a) the Seebeck and c) the Peltier effect. b) describes both effects in terms of density of states. Image taken from W. Germs [3].

The Seebeck effect occurs due to the temperature dependence of the Fermi level in the used material. A material with a fixed concentration of electrons and a density of states (DOS), which is not constant will have a temperature dependent Fermi level. When heating up one side of the used material, the Fermi level changes on this side, which can be measured as a thermo voltage. Hence,

$$\boldsymbol{V_t = S\Delta T} \tag{1}$$

with *S* being the Seebeck coefficient. The magnitude of the Seebeck coefficient is determined by the energy difference between the Fermi level and the states of the mobile charge carriers[3]. The Seebeck coefficient is calculated using the expression [3]

$$\boldsymbol{S = \frac{\int (E-E_f)\sigma(E)dE}{eT\int \sigma(E)dE}} \tag{2}$$

Which can be explained as the associated heat of a state *E-E$_f$* weighted by its contribution to the conductivity $\boldsymbol{\sigma(E)}$ and divided by the unit charge and the temperature. Here the conductivity is given by

$$\boldsymbol{\sigma(E) = e \cdot n(E) \cdot \mu(E)} \tag{3}$$

here *e* is the unit charge again, $\boldsymbol{n(E) = n_{doping}(E) + n_{sc}(E)}$ the total density of free charge carriers and $\boldsymbol{\mu(E)}$ the mobility of these charge carriers.

The Seebeck effect is the driving force behind thermoelectric generators. These TEG’s function like heat engines, but are less bulky, have no moving parts and are typically less efficient. When deriving the efficiency of a TE device, the figure of merit for TE devices can be found, this is done in

2.4 Derivation of the thermo electrical figure of merit. The figure of merit is defined in order to determine the relative usability of a material for application in a TEG. Since we want to use organic semiconductors to transfer heat into a thermo voltage, the figure of merit is a very important property for a material. The figure of merit is defined by

$$\boldsymbol{ZT = \frac{S^2\sigma}{\kappa}T} \tag{4}$$

Here σ is the electrical conductivity and κ is the thermal conductivity. The figure of merit can now be calculated at a certain temperature T. A higher value for ZT means a higher relative utility of a certain measured material in a TEG. For this report the focus will lay on optimising the so called power factor $S^2\sigma$, which in the optimal case would be high compared to κ. The following two paragraphs explain the electrical conductivity and the derivation of the figure of merit ZT.

2.3 Electrical conductivity

The easiest way to explain the electrical conductivity is by introducing it as the reciprocal of electrical resistivity. Electrical resistivity is an intrinsic property that quantifies how strongly a material opposes the flow of electrical current. Resistivity is commonly represented by the Greek letter ρ. Since conductors by definition conduct well, their resistivity is lower than the resistivity of insulators. Conductors typically have free charge carriers which can flow through the material, whereas in insulators the charge carriers are bound to their atoms. Usually the resistance *R* of a material is measured with Ohm's Law and by determining the geometry, length *l* and cross-sectional area *A* of said material, the resistivity can be calculated with the following equation:

$$\boldsymbol{R = \rho\frac{l}{A} = \frac{V}{I}} \tag{5}$$

The resistivity ρ is thus independent of the geometry of the measured material and is expressed in $\Omega \cdot m$. Since this is an intrinsic property, it has the same value for all objects made of the same material, independent of the shape of the object. The conductance of a measured material is now defined as

$$\boldsymbol{G = \frac{1}{R}} \tag{6}$$

The conductance *G* is the reciprocal of the resistance *R*, it is expressed in Ω^{-1} and is dependent of the shape of the measured material, just like its counterpart. Now the conductivity σ is the intrinsic property that quantifies how well a certain material conducts an electrical flow, independent of its geometry. As explained earlier in this paragraph, the conductance is the reciprocal of the resistivity in the same way that the conductance is the reciprocal of the resistance:

$$\boldsymbol{\sigma = \frac{1}{\rho}} \tag{7}$$

It does not require further explanation to say that the unit of σ is $(\Omega m)^{-1}$, or S/m where S is defined as Ω^{-1}.

2.4 Derivation of the thermo electrical figure of merit

The figure of merit Z was introduced by Ioffe[5] as a byproduct of the derivation of TE efficiency. The derivation is described in this section and proceeds[4] by considering the two-element generator shown in Figure 2.

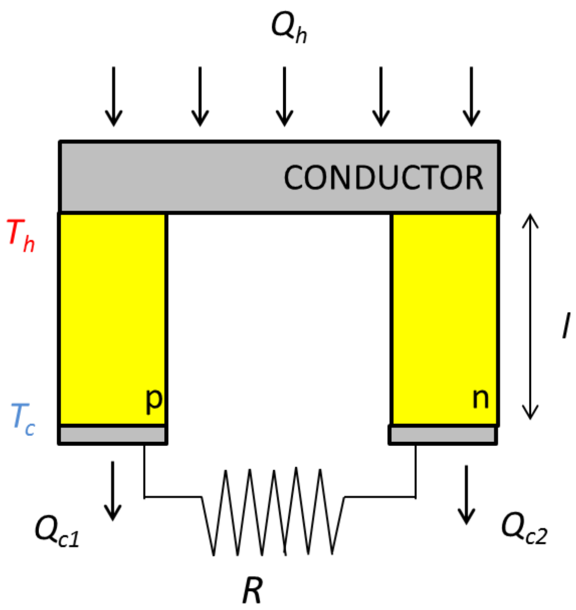

Figure 2 A two-element TE generator[4].

In above TEG an n-type and a p-type thermo element of length l are connected in thermal parallel and electrical series. The ingoing heat energy flux Q_h enters from the top of the generator. Heat energy fluxes Q_{c1} and Q_{c2} come out of the bottom of the device. The heat flux passes through the device, driven by the temperature difference T_h-$T_c > 0$. A conductor electrically connects the thermo elements. We assume this conductor has negligible electrical resistance and thermal resistance. Between the two thermo elements a load resistor R, representing the connected device, is connected.

In order to calculate the TE efficiency the following assumptions are made:

1. The electrical conductivity $\sigma_p = \sigma_n = \sigma$ over the temperature range $T_c \leq T \leq T_h$.
2. The thermal conductivity $\lambda_p = \lambda_n = \lambda$ over the temperature range $T_c \leq T \leq T_h$.
3. The Seebeck coefficient $S_p = -S_n = S$ over the temperature range $T_c \leq T \leq T_h$.
4. $A_p = A_n = A$ is the cross-sectional area of the thermoelements.

For a number a of thermo elements, half of which are n-type and half of which are p-type, the total internal electrical resistance (here called r), thermal conductivity and generated voltage are, respectively,

$$\boldsymbol{r = \frac{al}{\sigma A}}, \ \boldsymbol{\kappa = \frac{a\lambda A}{l}} \qquad \text{and} \qquad \boldsymbol{V_{OC} = aS(T_h - T_c) = S'\Delta T} \qquad (8)$$

Maximizing power output

Firstly we will determine the maximum power output of this TE generator, so we need the electrical current and power delivered to the external load *R.*

$$\boldsymbol{I = \frac{V_{OC}}{r+R} = \frac{S'\Delta T}{r+R}} \quad \text{and} \quad \boldsymbol{W = I^2 R = \frac{S'^2 \Delta T^2 R}{(r+R)^2}} \tag{9}$$

Differentiating *W* with respect to *R* gives us the value of load resistance that yields the maximum output power. Doing so we obtain

$$\boldsymbol{R_{P_{MAX}} = r} \tag{10}$$

By substituting *R* = *r* into eq. $\boldsymbol{I = \frac{V_{OC}}{r+R} = \frac{S'\Delta T}{r+R}}$ and $\boldsymbol{W = I^2 R = \frac{S'^2 \Delta T^2 R}{(r+R)^2}}$ (**9**
and using the definition of the internal resistor *r* we obtain an expression for the maximum power that can be generated from the given TE device:

$$\boldsymbol{W_{MAX} = \Delta T^2 \times \frac{aA}{4l} \times \sigma S^2} \tag{11}$$

Divided in these three terms we can easily see the dependence of the maximum power output upon the temperature difference. The second term expresses the dependence upon the way the device is constructed and the amount of thermo elements. The third term describes dependence on the so called power factor σS^2. Since this is an ideal model of a TE generator we find that the thermal conductivity λ has no direct impact on the maximum power output of the device. However, in practical generators there will be nonzero thermal resistances connecting the thermoelements to the thermal reservoirs, resulting in an influence of λ on ΔT.

Maximizing efficiency

The consumed energy[4] is the heat energy entering the hot junction and is given by

$$\boldsymbol{Q_h = \kappa \Delta T + S' T_h I - \frac{I^2 r}{2}} \tag{12}$$

Here the first term describes the heat flux transferred from the hot junction to the cold junction, the second term describes energy transport due to the Peltier effect. The third term describes the generated Joule heat, of the total Joule heat $I^2 r$ half passes through the hot junction and the rest is transferred to the cold junction.

If we now define

$$\boldsymbol{m = \frac{R}{r}} \tag{13}$$

and use the expressions from eq. $\boldsymbol{I = \frac{V_{OC}}{r+R} = \frac{S'\Delta T}{r+R}}$ and $\boldsymbol{W = I^2 R = \frac{S'^2 \Delta T^2 R}{(r+R)^2}}$
(**9** we derive the efficiency of the generator as

$$\boldsymbol{\eta = \frac{W}{Q_h} = \frac{\Delta T}{T_h} \times \frac{\frac{m}{m+1}}{1 + \frac{\kappa r (m+r)}{S'^2 T_h} - \frac{\Delta T}{2T_h(m+1)}}} \tag{14}$$

Now we define

$$\boldsymbol{Z = \frac{S'^2}{\kappa r} = \frac{\sigma S^2}{\lambda}} \tag{15}$$

We note that *Z* is solely dependent of material properties. The product *ZT* is dimensionless and is often used as a quality measure for a TE material. *ZT* is called the figure of merit for thermo electrical devices.

Now we can express the efficiency as a function of the hot and cold temperatures, T_h and T_c, and the parameters *m* and *Z*:

$$\boldsymbol{\eta = \frac{W}{Q_h} = \frac{\Delta T}{T_h} \times \frac{\frac{m}{m+1}}{1+\frac{m+1}{ZT_h}-\frac{\Delta T}{2T_h(m+1)}}} \tag{16}$$

If we now maximize η with respect to *m* we find

$$\boldsymbol{R_{\eta\max} = rm = r + \sqrt{1+ZT}} \tag{17}$$

where $T = \frac{T_h - T_c}{2}$. Substituting eq. 17 into eq. 16 yield the maximum possible efficiency for any TE generator that is built using materials with a given *Z*

$$\boldsymbol{\eta_{max} = \frac{\Delta T}{T_h} \times \frac{\sqrt{1+ZT}-1}{\sqrt{1+ZT}+\frac{T_c}{T_h}}}. \tag{18}$$

This result means that, for constant TE parameters, the maximum efficiency with which any TE generator can extract energy from a temperature difference is dependent only upon T_h, T_c and *Z*. If we for instance let *Z* go to infinity we find that the maximum efficiency of our TE device is the Carnot efficiency.

2.5 Organic electrochemically gated transistors

One way of controlling the power factor $S^2\sigma$ is by using controlled doping. In an organic semiconductor, doping and gating moves the Fermi level to a higher energy, which may greatly increase the number of filled states. This changes the electrical properties of the used device. By doping the material the Fermi level will rise, moving it higher up the Gaussian shaped conduction band. The way the DOS of this conduction band is shaped greatly influences the effect this has upon the Seebeck coefficient and the conductivity. A schematic representation of the shape of this band is shown in Figure 3.

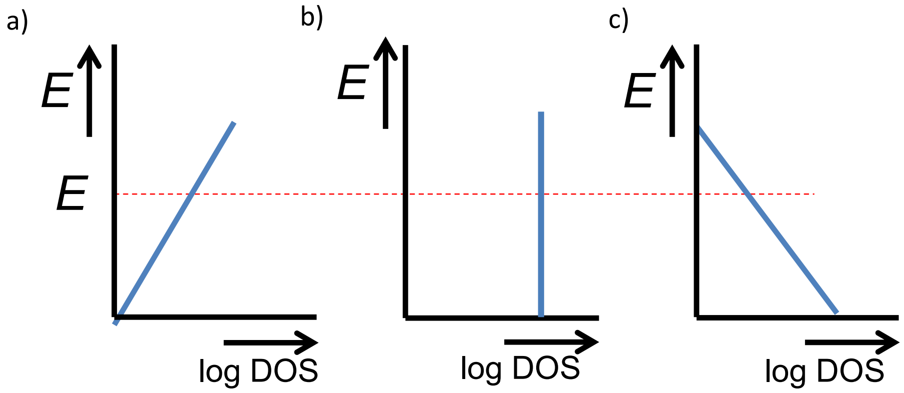

Figure 3 Representation of the Gaussian DOS model. a) The lowest part of the conduction band. The DOS of the lower part of the conduction band is approximated as being exponentially increasing, the states of the DOS will be partially filled up to the Fermi level. b) At some point moving higher up the band the DOS will be constant, on top of the Gaussian shape. c) At the top of the conduction band the DOS will decrease exponentially, mirroring the bottom tail of the Gaussian shape.

The conductivity is highly dependent on the amount of free charge carriers in the material. Since only the electrons near the Fermi level E_f are not localized and thus can contribute to the conductivity of the material, increasing the Fermi level can have a sizeable effect on the conductivity. Doping a material with charge carriers increases the Fermi level, which in region a) shown in Figure 3, results in an increasing conductivity. An increasing conductivity σ has of course a positive effect on the powerfactor $S^2\sigma$ and hence on the figure of merit following eq.$\boldsymbol{ZT}$=$\boldsymbol{\frac{S^2\sigma}{\kappa}T}$ (**4**. Doping the material also has an effect on the Seebeck coefficient, this dependence is best explained using equation $\boldsymbol{S = \frac{\int (E-E_f)\sigma(E)dE}{eT\int \sigma(E)dE}}$ (2.

$$S = \frac{\int (E - E_f)\sigma(E)dE}{eT\int \sigma(E)dE}$$

So the magnitude of S is determined by the energy difference between E_f and the energy E of the transporting states. By doping the material, i.e. increasing the charge density, the Fermi level rises, so the heat transport by the carriers $(E - E_f)$ decreases. Consequently a lower S and a lower power factor will be observed. So on one hand doping increases σ and on the other hand it lowers the magnitude of S. Using controlled doping, we hope to find out what the resulting effect is of doping on the power factor $S^2\sigma$.

3 Experimental setup

The research described within this report is divided in two fields: Measurements on the Seebeck coefficient and measurements on organic electrochemically gated transistors. In this chapter the setup used for the Seebeck measurements is explained in detail. Furthermore, the different kinds of used samples are described in this chapter.

3.1 Seebeck measurements

The measurement setup used for the Seebeck coefficient measurements is shown in Figure 4[2].

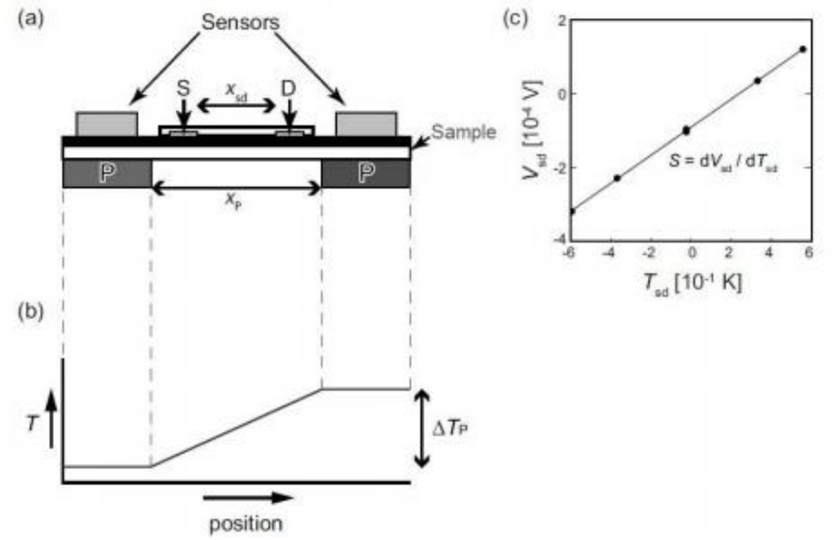

Figure 4 a) Representation of the setup used for Seebeck measurements. b) The assumed constant temperature gradient created by the Peltier elements. c) A linear fit of the voltage over the source and the drain *V_{sd}* as a function of the temperature difference between source and drain ΔT_{sd}

The source **S** and drain **D** electrodes are placed on the sample. Two Peltier elements **P** generate a constant temperature gradient between the source and drain side of the sample, explained later this section. Two Silicon diode **sensors** on top of the sample measure the temperature *T* on either side of the sample. Since the temperature gradient is estimated as being constant as shown in Figure 4b), the temperature at the two ends of the sample is enough to know the whole temperature profile. The temperature difference between the source **S** and drain **D** is calculated from the temperature difference between the **P**eltier elements ΔT_p, the distance between the Peltier elements x_p, and the distance between the source and drain x_{sd}:

$$\Delta T_{sd} = \Delta T_p \cdot \frac{x_{sd}}{x_p} \tag{19}$$

Calculating the slope of the graph shown in Figure 4c) now yields the Seebeck coefficient *S*, ***Vt=S*ΔT** (**1**. When the temperature difference between source **S** and drain **D** is varied and for each constant temperature gradient the voltage V_{sd} is varied along a sweep, we can calculate the Seebeck coefficient of the used sample.

Peltier elements

The Peltier elements create a temperature difference between the source and the drain electrode[2]. These elements are based on the Peltier effect, introduced in section

2.2 Seebeck-Peltier effect. When sending a current through a Peltier element, it heats up on one side and cools down on the other depending on the Peltier coefficients of the used materials. The Peltier coefficient is defined as the heat carried per unit charge and is related to the Seebeck coefficient following:

$$\boldsymbol{\Pi} = \boldsymbol{S} \cdot \boldsymbol{T} = \frac{\int (\boldsymbol{E}-\boldsymbol{E_f})\boldsymbol{\sigma}(\boldsymbol{E})\boldsymbol{dE}}{\boldsymbol{e}\int \boldsymbol{\sigma}(\boldsymbol{E})\boldsymbol{dE}} \tag{20}$$

A schematic representation of a Peltier element is shown in Figure 5[2]. Two types of (inorganic) semiconducting materials, one n-type (A) and one p-type (B), are placed in series. These two materials have a Π that is either positive or negative. By alternating between n- and p-type materials, for a given current direction the n- and p-legs heat up at the same side. For the current direction shown in the figure below, the upper surface of the Peltier element is heated and the lower surface is cooled down.

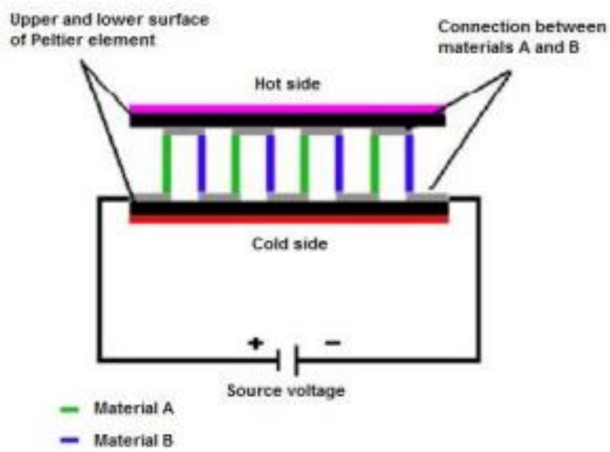

Figure 5 Schematic representation of a Peltier element. When a voltage is put over an altering row of two materials A and B, a temperature difference between the two surfaces of a Peltier element arises.

When two Peltier elements are placed on a sample holder, the holder will have a constant temperature after a settling time t_{settle} as long as the holder is large enough and can conduct heat well enough. In that case the holder works as a heat bath.

3.2 Samples

A schematic image of the samples that are used in the measurements is shown in Figure 6. The sample firstly consists of a glass substrate. The substrates were cleaned by sonication in successively water-soap, water, and 2-propanol baths. After drying, the substrates were placed in a UV-ozone cleaner for 20 min. Upon the substrate either a layer of PEDOT:PSS, PPV or F8BT is spin-coated with a velocity of 1000 RPM. On top of this golden electrodes are damped.

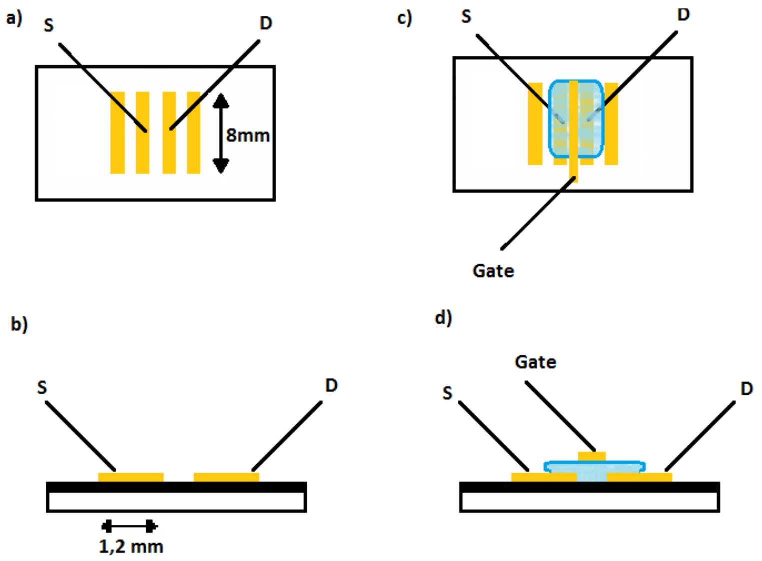

Figure 6 A schematic representation of the used samples with the used probe needles (black lines with letters). a) Shows a top view of the samples used in the Seebeck measurements. b) The Seebeck sample shown from the front side. From the bottom up it is a glass substrate with a thickness of 1mm, the transparent active layer of (50-150)nm shown in black and then the golden electrodes (70nm). c) Samples used in the doping measurements, the blue figure on top of the sample represents a droplet of dried electrolyte. d) The front side of the doping sample. The gate is placed in the middle between S and D.

In a measurement a probe needle, shown by a black line, is placed on each electrode. The contact between the electrode and the probe needle is enhanced by some silver paste on the surface of the electrode. We used the middle two electrodes that are shown in Figure 6a). These electrodes are x_{sd} = 1 mm apart, making the canal in which the current flows through the active layer have a cross-sectional area of $A = t_l \cdot 7$mm, here t_l is the thickness of the active layer. The canal length has been varied for the doping measurements. In this case thin wires of varying thickness were placed in the middle of the template before damping on the electrodes, resulting in a thin canal between the two electrodes. So the two electrodes in Figure 6c) are typically less than 0,15 mm apart. To prevent confusion in interpretation, the canal is not shown as thin in the figure.

As previously mentioned, several materials have been measured. The active layers we have used are several different (semi)conductive polymers named PEDOT:PSS (type PH1000) and PPV for Seebeck measurements and F8BT for doping measurements. Also the thickness of these active layer was varied between different samples, of course this varying cross-sectional area *A* was taken into account when calculating for example the conductivity. For the doping measurements we used an electrolyte based on PEO with KTF, on the early doping experiments we have dissolved these in acetone, later acetonitrile was used since ACN contains less water and because of that has less chance of side reactions.

4 Preliminary Experiments

Before starting the experiments where controlled doping is used, some preliminary experiments took place. In this chapter the Seebeck measurements will be discussed first. Next the preliminary doping experiment is discussed, being a simple gate saturation experiment. To end this chapter an overview of the used LabVIEW program, used to perform the doping measurements, is presented. LabVIEW is also used for the Seebeck measurements, the script used for that experiment is explained in [2].

4.1 Seebeck experiment

The Seebeck experiment can be divided into several measurements, firstly the temperature settling measurement which provides an insight in the settling time of the temperature after a temperature step. After the temperature is settled, the bias voltage (or voltages) is swept from a positive bias to a negative bias. The results of the measurements of these sweeps lastly provide the required information to calculate a Seebeck coefficient for the used device.

4.1.1 Temperature settling measurement

As described in the experimental setup, two Peltier elements were used in the Seebeck measurements to provide a constant temperature gradient over the used sample. This change in temperature of both sides of the sample takes place before a voltage sweep. Using two silicon diode sensors this temperature difference on both ends of the sample is measured. The time settling measurements take place to get insight in how the temperature behaves after providing the Peltier elements with a constant current.

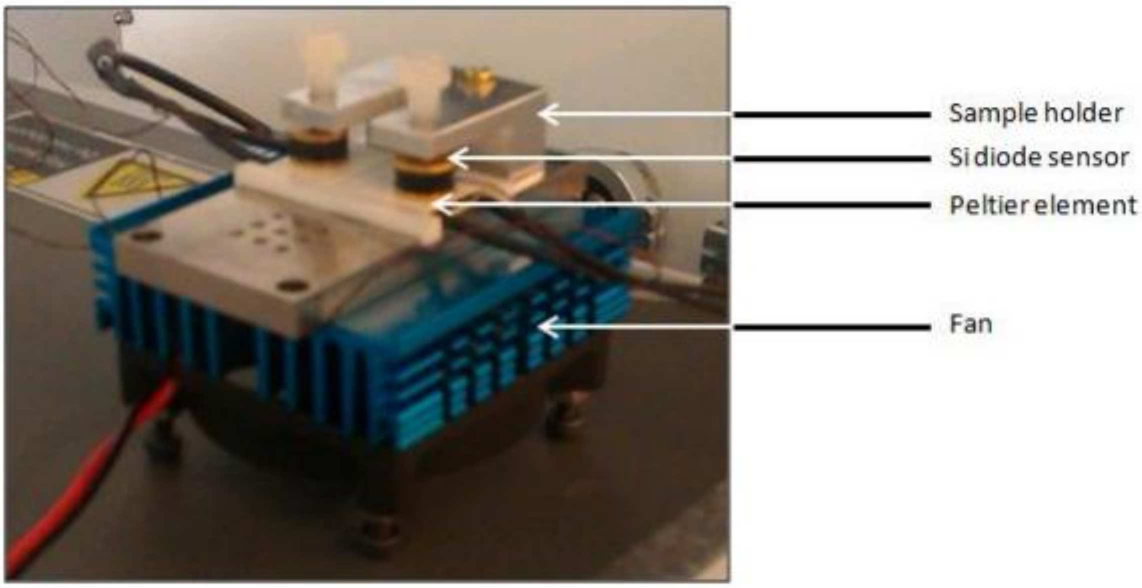

Figure 7 The measurement setup used for the Seebeck measurements [2]. On top of the white Peltier elements a sample was mounted during measurements. Between the sample and the Peltier elements a gel was used to improve thermal contact. The Si-diode sensors were placed upon the sample and the white screws above them were used to push them against the sample. Four probe needles were placed upon the sample electrodes as explained in section 3.2 Samples.

At the start of a temperature step, i.e. after a current step towards the Peltier elements, it is expected that the temperature measured by the Si-diode sensors will rise or decay rapidly. After about 180 seconds this rapid decay/rise should curve towards ideally a constant temperature[2]. Then the rest of the Seebeck measurements can take place at a constant temperature gradient as shown in Figure 4b). Every change of temperature in the Seebeck experiments is accompanied by a file which describes the settling of the temperature, one example of a temperature settling measurement is show in the figure below.

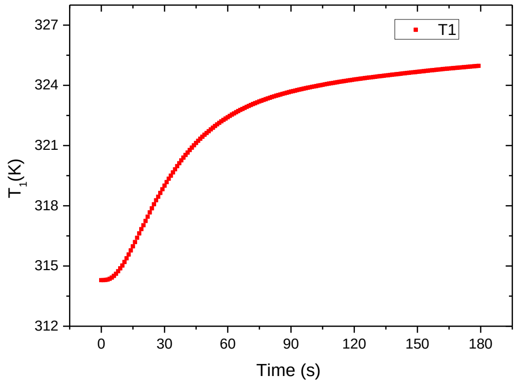

Figure 8 An example of a temperature settling curve. At *Time* = 0s a step in the current sent through the Peltier elements takes place. The increasing current corresponds to a step in temperature *T* from 313K to 324K. As expected the increase of temperature starts out rather steep and afterwards moves towards a constant value.

The graph of the temperature settling shows the expected behaviour. It does not reach a constant temperature yet after 180 seconds. This is of course not ideal, and it is the reason the temperature at both sides of the sample is measured while performing the subsequent voltage sweeps. These measurements yield a maximum temperature variance of less than dT = 0,5 K, which is taken into account when calculating the Seebeck coefficient.

4.1.2 Voltage sweeps

After the temperature is settled, the bias voltage (or voltages) are swept from a positive bias to a negative bias using the two probe needles. This results in a linear response of the measured current between source and drain. In this section the results of the voltage sweeps on PEDOT:PSS are explained.

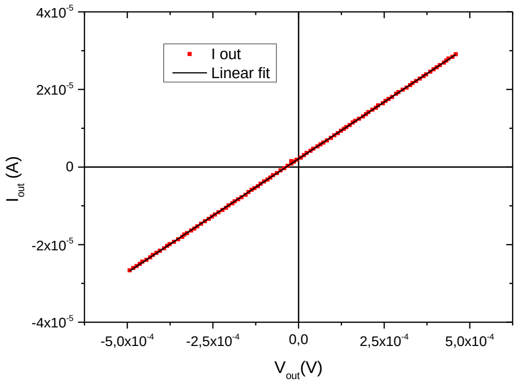

Figure 9 A result of a voltage sweep on PEDOT:PSS. The slope of this measurement is $\frac{dI}{dV}$ and is equal to the conductance of the material. For instance the slope of the linear fit is *G* = (5,86±0,01)·10^{-3} S.

For the type of measurement displayed above one of the four probe needles provides a bias voltage V_{bias} , one probe measures the out coming voltage V_{out} and provides a grounding. Now the out resulting current I_{out} is measured. Plotting I_{out} against V_{out} results in the graph above. The found slope is equal to the conductance *G* in accordance to equation $\boldsymbol{R}= \boldsymbol{\rho}\frac{\boldsymbol{l}}{\boldsymbol{A}}=\frac{\boldsymbol{V}}{\boldsymbol{I}}$ (**5** and $\boldsymbol{G}=\frac{\boldsymbol{1}}{\boldsymbol{R}}$ (**6**. Since the cross-sectional area of the channel through which the current flows through the active layer is known, the conductivity σ can be calculated. Because of the temperature difference applied over $Vt=S\Delta T$(equation $\boldsymbol{Vt=S\Delta T}$ (**1**), this explains the offset of the graph. Now this offset, so V_t is obviously equal to the value of *V* where I_{out} is equal to zero, so the intersection of the fit with the x-axis. During the measurement above also the temperature is $\boldsymbol{Vt=S\Delta T}$ (**1** the Seebeck coefficient can easily be calculated for every voltage sweep, with its according temperature difference.

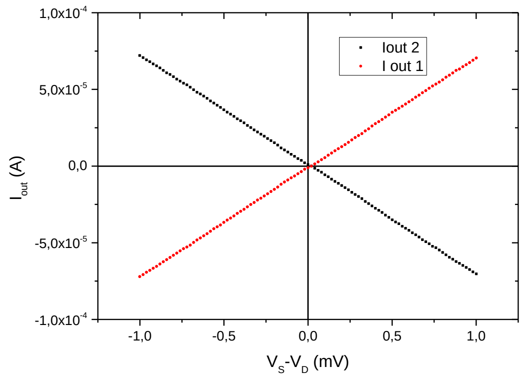

Figure 10 A voltage sweep using the Dualbias program. For both electrodes these measurements use a double, opposite bias voltage with respect to a ground. Here the slope is G = (3,57±0,03)·10^{-2} S.

The dual biased measurements shown in the figure above enjoy the same processing as the previously shown measurements. The difference is that here I_{out1} equals -I_{out2}, resulting in the two linear fits that intersect with each other and the x-axis in V_t. Reason for the seemingly unnecessary effort put into the "extra" linear fit comes when the doping experiment begins. Here leakage currents come into the picture. In the case of the first type of sweeps, a leakage current that contributes to the measured source-drain current would result in a fit that wouldn't intersect with the x-axis in V_t anymore, but rather in a completely different V. The dual biased system has the advantage that the leakage current that occurs with the doping experiment would contribute to both I_{out1} and -I_{out2}, resulting in the two fits forming a cross that doesn't intersect the x-axis in its centre. However, since the intersection of both fits has only shifted vertically, the thermo voltage can be derived from this intersection.

4.1.3 Results and discussion

We are interested in the Seebeck coefficient which is the thermo voltage that occurs when a temperature difference of one Kelvin is applied over the sample. The above experiments yielded series of V_t and their corresponding ΔT. When plotting the arisen thermo voltages against the temperature differences the slope of the linear plot is the Seebeck coefficient S. An example of such a graph is shown in the figure below.

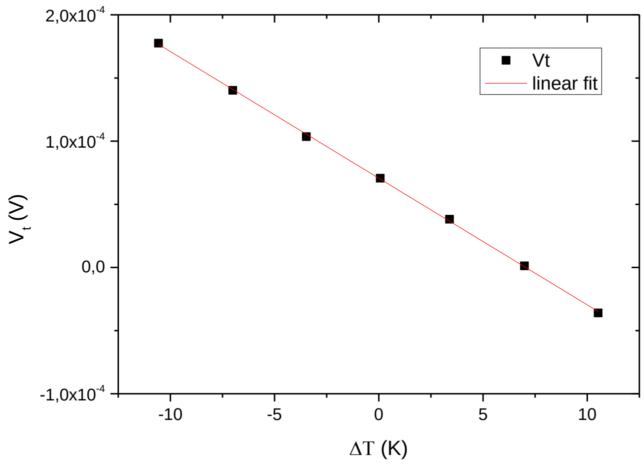

Figure 11 An example of a $V_t - \Delta T$ plot of a PEDOT:PSS sample. The polarity of the slope of this graph is determined by the definition of the temperature difference over the sample. The slope of this curve yields a Seebeck coefficient of *S* = (10,03±0,07)µV/K.

The Seebeck coefficients we found for the PEDOT:PSS are in the order of $S = 10^{-5}$ V/K. this value can be expected when looking at previous results in literature. As explained previously, also the conduction of the samples has also been calculated, meaning the conductivity σ is now easily calculated when the geometry of the used sample is known. The shown measurements of both Figure 9 A result of a voltage sweep on PEDOT:PSS. The slope of this measurement is $\frac{dI}{dV}$ and is equal to the conductance of the material. For instance the slope of the linear fit is G = (5,86±0,01)$\cdot 10^{-3}$ S. and Figure 11 come from a single PEDOT:PSS sample, which seems to me measured with just a slight error. When using 68% statistics we find for the conductivity σ = (1,673±0,001)S/m and as shown above S = (10,03±0,07)µV/K. These values correspond with previous experiments found in literature [6,7].

4.2 Preliminary doping experiments

Before commencing the controlled doping experiment, a LabVIEW script has been written to control the measurements. All of the measurements that are performed in this chapter are computer-controlled. LabVIEW is a graphic program, used by many engineers and scientists, which can control and read out hardware like voltage sources or function generators. Also the gate saturation has been measured, this is expressed in the time it takes for the gate current to become constant after a step in gate voltage.

4.2.1 LabVIEW

The measurements performed in these experiments are computer-controlled using LabVIEW. LabVIEW is a graphical programming platform that helps engineers and scientists control and read out hardware. It provides an interface in which the different components used in the setup can be controlled and it reads out the measurements done by these components to save these in text files.

For the doping measurements the LabVIEW program is used to develop a program that contains the drivers for two Keithley 2636A System Sourcemeters. For the measurements the first Sourcemeter has two probe needles connected to it and is used to sweep the source-drain voltage and measure the currents at the source and drain electrodes described in section 3.2 Samples The second Sourcemeter is connected to the third probe needle and is used to apply the gate voltage and measure the gate current.

The program written in LabVIEW is made so measurements are made following the protocol schematically shown in the figure below.

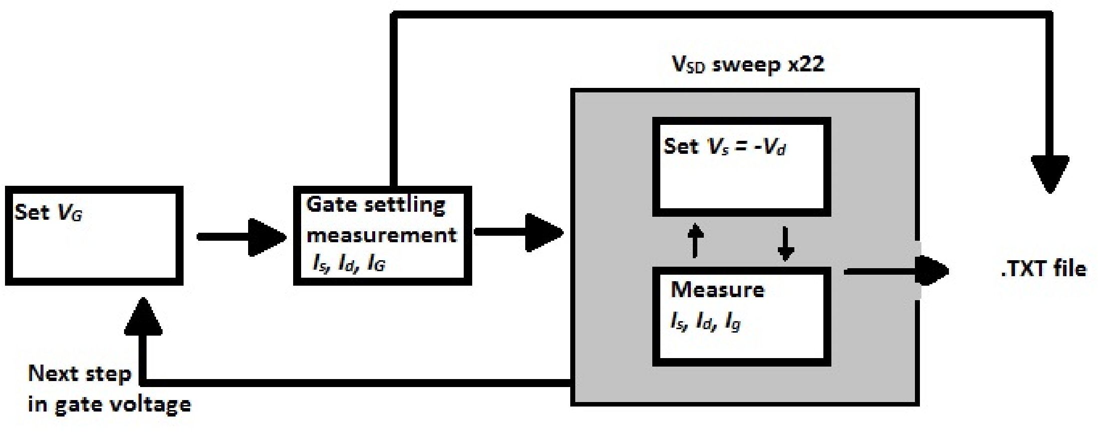

Figure 12 A schematic representation of the LabVIEW program written for this experiment.

First a gate voltage V_G is set on the gate electrode with respect to a ground. Directly after this measurement the gate, source and drain current are measured for a certain amount of time t_{settle}, specified by the user. These measurements are saved in a text file. When the settling time is over, the source and drain voltages are set for V_s=-V_d. After measuring the gate, source and drain current the source and drain voltage are set to the next value, to repeat itself all over. The range of values of V_s=-V_d is specified by the user, this range is then divided into 22 even steps, making the loop repeat itself 22 times. When this V_{sd} sweep across all 22 values is measured and sent to a text file, the next step in gate voltage is set by the first sourcemeter.

An interface is made for this program in which the user can specify the parameters for the measurements. In this front panel the user specifies the range of gate voltages and the saturation time after each V_g step, also the number of steps is given by the user. Apart from this the maximum source-drain voltage is inserted by the user, this maximum voltage is divided into 22 even steps by the program, together being one V_{sd} sweep. Furthermore V_{sd} during doping (while gate settling) can be changed in the front panel.

4.2.2 Gate saturation measurements

In the controlled doping experiments a dielectric is placed on the samples, with on top of the dielectric a gate electrode, making the sample an organic electrochemically gated transistor. The setup of such a sample is schematically represented in the figure below.

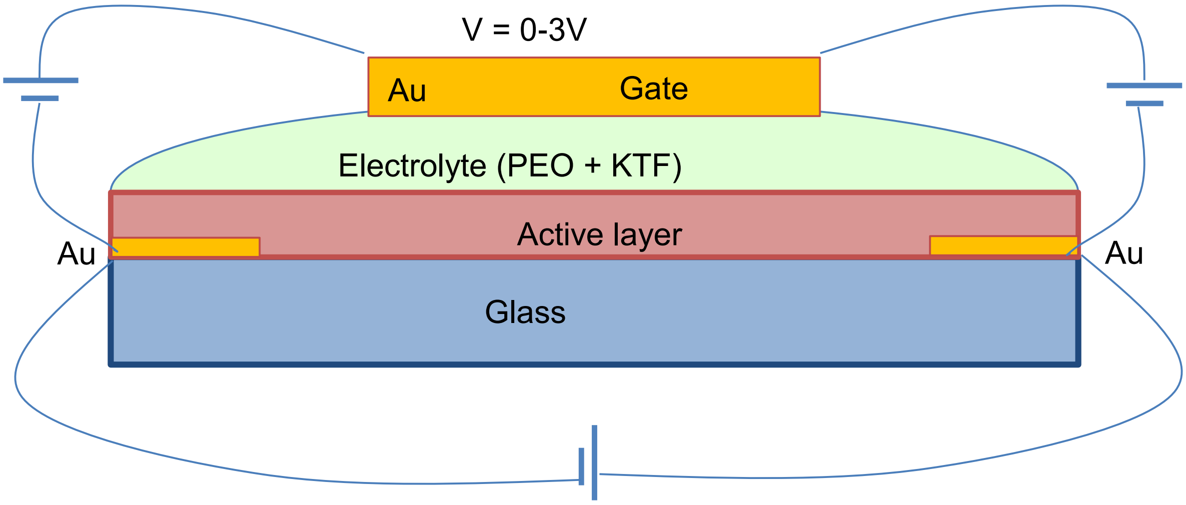

Figure 13 Schematic representation of the organic electrochemically doped transistor setup of the used samples. The gold electrodes on the left and right hand side are used as source and drain electrode.

The representation is not scaled and is purely sized for clarity. The measures of the real samples are discussed in section 3.2 Samples. The gate voltage has a maximum of V_G = 3 V because above this voltage the salt in the electrolyte may oxidize or reduce. During the experiment the gate voltage varies between 0 V and 3 V in steps. After every step the gate current needs some time to settle, analogue to the temperature settling in section 4.1 Seebeck experiment. After a step in gate voltage the system goes to an equilibrium where I_{sd},I_{sg} and I_{dg} are constant, then the V_{sd} sweep described in 4.1.2 takes place. As explained in said section the dual bias sweep will be performed. The gate saturation measurement is displayed in the next figure.

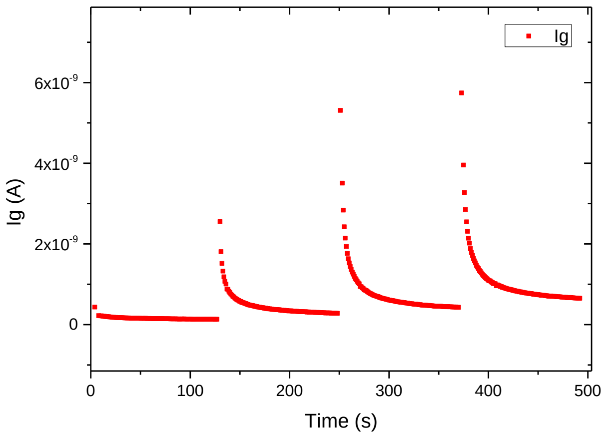

Figure 14 The gate saturation measurement upon changing the gate voltage. Every 120 seconds a step in gate voltage is performed, resulting in the gate current settling to a constant value.

As shown in the above figure the gate current peaks when a gate voltage step is being made. After this peak it slowly settles to a constant value. The settling time is taken to be 120 seconds, for it has almost reached its constant state. Of course it would be ideal to wait longer, so the gate current will not vary while measuring the V_{SD} sweep. However, since the voltage changes 20 times per measurement series, one minute of extra settling time would already result in 20 minutes extra duration per measurement.

5 Results and discussion

In this section the results of the controlled doping experiments on the described organic electrochemically gated transistors are displayed and discussed. Three different types of devices are measured and discussed in this chapter. The first discussed series of samples has an active layer consisting of Super-Yellow PPV with an electrolyte based on PEO with KTF dissolved in acetone (as described in 3.2). The second series of samples consists of F8BT and the same electrolyte. The third described series of samples also contains F8BT, but in this series the electrolyte is dissolved in acetonitril. Each section starts with some typical measurements for the series, after these the results are displayed and discussed.

5.1 Super-Yellow PPV series

The first series of samples has an active layer consisting of Super-Yellow PPV, the samples enjoy an electrolyte based on PEO with KTF dissolved in acetone. To fully understand the results it is necessary to first exhibit some measurements from samples out of this series.

5.1.1 Measurements

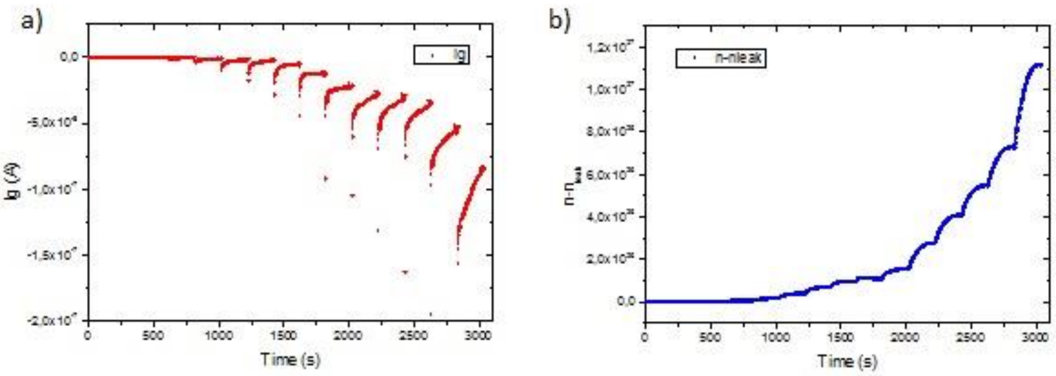

Figure 15 Measurements performed on a sample with an active layer consisting of SY PPV. a) The gate current is measured during the gate saturation measurements described in 4.2. b) The resulting doping density is displayed.

The doping density n-n_{leak}, shown above, is calculated out of the gate current and the estimated leakage current. Firstly the leakage current is determined. The leakage current is expected to be constant for a certain V_g , since it has settled for two minutes as described in section 4.2 Preliminary doping experiments and is estimated to be the last value of I_g before the next gate voltage step takes place. When integrating the gate current (minus the estimated leakage current) over time, we find the total amount of charge in the active layer. Dividing this by the elemental charge and of course the geometry of the sample, we find the doping density.

5.1.2 *Results and discussion*

Not only the doping density has been calculated from the measurement. Also the conductivity and mobility are calculated. Each of the measured electrical properties is displayed in the following figure, next to each of the results a description is provided of the executed calculations.

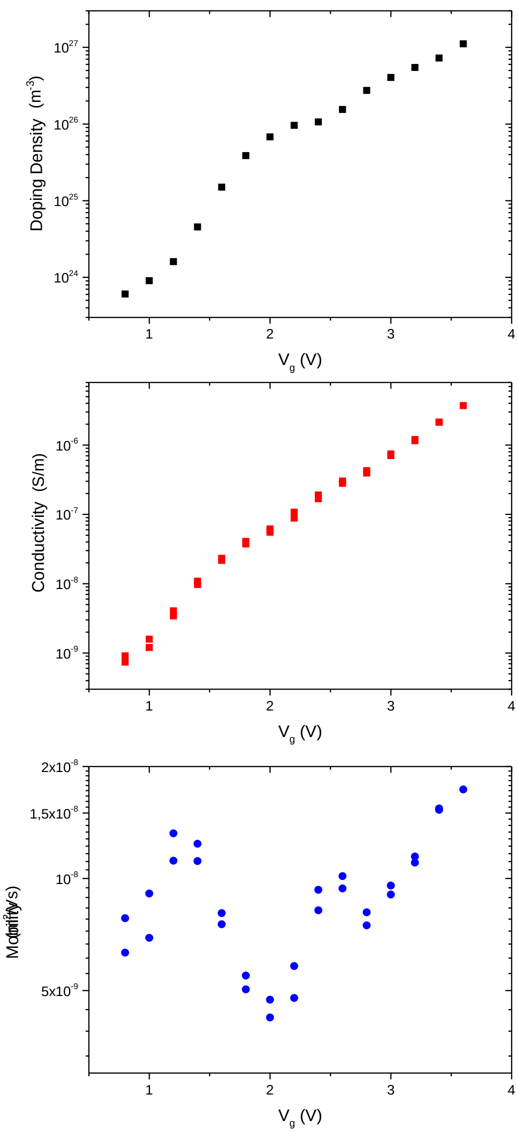

Figure 16 The results of the measurements done on a SYPPV sample. In these measurements some insulating tape is used to minimize leakage current between gate and source - drain electrodes.

The **doping density** rises when increasing the applied gate voltage. When applying a higher voltage to the gate electrode, its voltage difference compared to the active layer will of course increase. Because of this voltage difference charge carriers will be injected into the active layer, in this case the PPV, thus doping the material.

The **conductivity**, displayed on the left, increases when raising the applied gate voltage. When applying a higher gate voltage, more free charge carriers are injected into the active layer, corresponding to the Fermi level rising as described in section 2.5 Organic electrochemically gated transistors. This results in a growing conductivity of the material. The described decrease in conductivity that may take place on the top of the conduction band is not witnessed in measurements on this series.

The **carrier mobility** is calculated out of the doping density and the conductivity. It is expected[10] to rise for a higher gate voltage. When the Fermi level rises and more delocalised charge carriers emerge in the material, the mobility of the charge carriers should also increase. In the graph shown on the left this is not the case, however the found carrier mobility does generally correspond to the mobility values found for SYPPV in literature[8][9].

5.2 F8BT – first series

The devices in this measurement series are organic electrochemically gated transistors with an active layer consisting of F8BT, with an electrolyte based on PEO with KTF dissolved in acetone. In these experiments the way of measuring is the same as described in the previous section. Just like in the previous measurements, insulating tape was used to shield the source and drain electrodes from the drain electrode, to minimize leakage current. The active layer is now F8BT, because the conductivity and mobility are expected to be more responsive to the doping in the sense that higher values may be achieved for both σ and μ, compared to Super-Yellow PPV. As before, this section starts out with several measurements.

5.2.1 *Measurements*

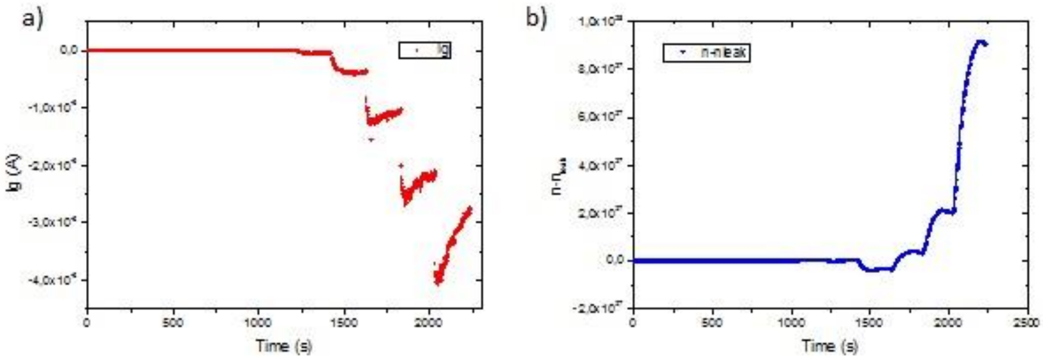

Figure 17 a) A typical gate settling measurement for the first F8BT series where the gate current plotted against the time. The negative gate voltages correspond to p-type doping. b) The calculated doping density.

The above figure displays unexpected behaviour by the doping density. The doping density is calculated from the gate current in accordance to the description in the previous section. The mentioned unexpected behaviour is the doping density n-n_{leak} decreasing for an increasing gate voltage. Reason for this result is the perturbation in the left graph, which gives a high uncertainty in the determination of the leakage current. In this care the leakage current was estimated too high, resulting in a calculated doping density that is lower than the actual doping density.

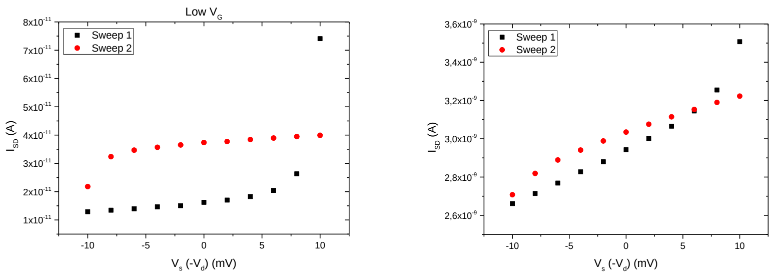

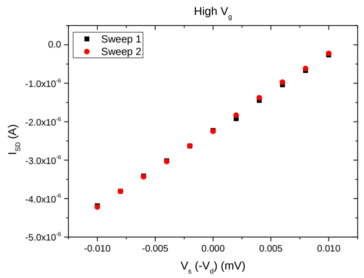

Figure 18 I_{sd} plotted against V_s for a low gate voltage (top left), a high gate voltage (bottom left) and a gate voltage in between (top right). The black sweeps start for a positive Vs and the red for a negative Vs, hence an effect originating from hysteresis is shown on two different sides and with opposite sign. This effect occurs in all measurements with samples from both F8BT measurement series and will be discussed in next section.

5.2.2 Results and discussion

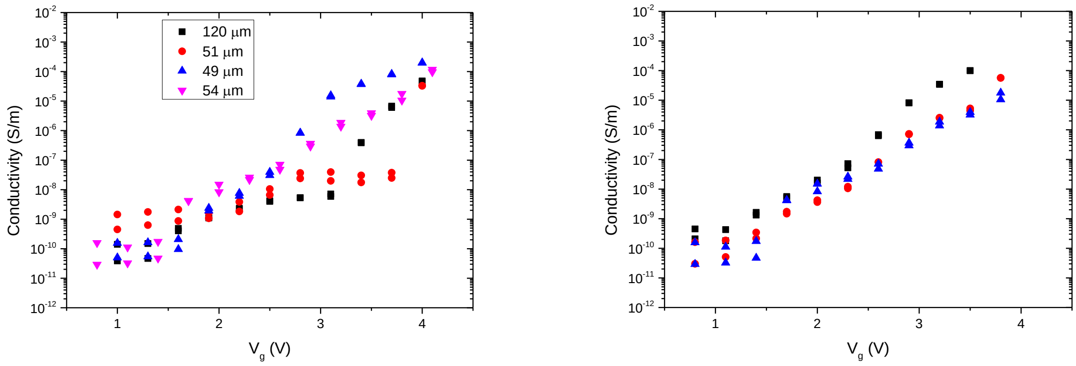

Figure 19 A summary of the measured conductivity of the first F8BT series. The calculated conductivity achieved a higher value than in the Super-Yellow PPV samples discussed in the last section.

The **conductivities** originate from the source-drain voltage sweeps shown in Figure 18. The voltage is swept subsequently upwards and backwards, resulting in two sweeps from which two conductivities can be calculated when taking into account the geometry of the canal. Since we now find 2 conductivities per gate voltage, we can compare these two values in order to see whether the 'upwards conductance' corresponds with the 'backwards conductance'. In the above results, this correspondence is expressed in the two resulting points of the conductivity (for the same gate voltage) overlapping.

For low values of the gate voltage, the source-drain current is relatively low compared to leakage current due to the gate current. This results in a clearly visible, but nearly constant, offset in the two I-V sweeps. Since the offset is constant, the two sweeps appear practically parallel, which would of course result in the two fits having a similar slope. A similar slope would of course yield a similar value for the calculated conductance. This is however not the case, because of the peculiar measured value of current at the start of both sweeps. The black sweep starts at $V_S = 1\text{mV}$, while measuring a much higher conductivity than expected. This high conductivity value is a product of hysteresis. Hysteresis is the dependence of the output of a system not only on its current input, but also on its history of past inputs. The offsets in the first measured values occur purely because of a dynamic lag between input and output. The output current lags behind, so to say. This effect would disappear as the input changes more slowly, which is referred to as rate-dependent hysteresis. As a result of the rapidly changing electric field we measure a current on top of the “real” source-drain current, due to the hysteresis that occurs. One can expect that this one measurement per sweep has a substantial influence on the calculated slope of the *I-V* fit, this results in the two different calculated slopes, and thus the different calculated conductivities for low V_G. As seen in the two other displayed voltage sweep measurements in section 5.2.1, the higher measured current due to hysteresis as well as the leakage current have a decreasing effective influence on the slope of the sweeps for higher V_g and thus higher values of I_{sd}. This corresponds to the results shown above in Figure 19, since for higher values of V_g the conductivities for the two sweeps are similar, resulting in overlapping points in the graphs. Another source of deviation from the expected behaviour of the sweeps can be attributed to the gate current not being constant. As explained in 4.2 Preliminary doping experiments, the gate current is not completely settled when the source-drain sweep starts, resulting in slightly deviating slopes of the two sweeps as seen in **Error! Reference source not found.**.

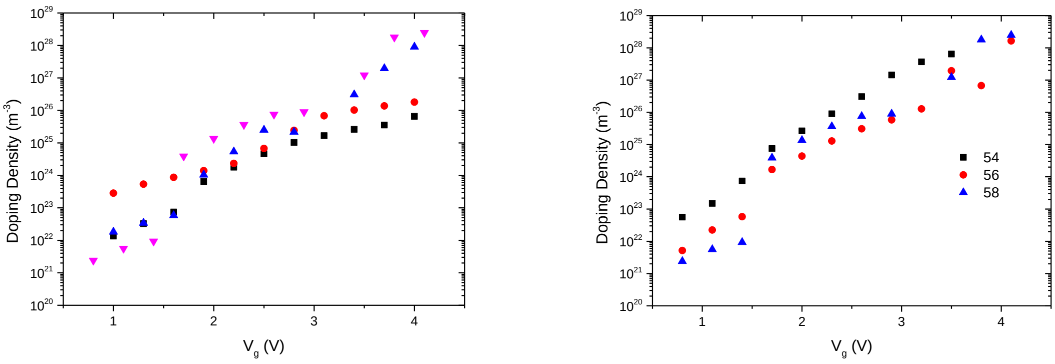

Figure 20 A summary of the doping density calculations on the first series of F8BT measurements.

The found **doping densities** n_{doping} in the F8BT layers are shown in above figure. These results originate from measurements as shown in Figure 17. Examining that figure shows us that for higher magnitude of time and thus V_g, the measured gate current gets less fluent and more noisy. When manually estimating the leakage current I_{leak} for lower V_g and comparing it with I_{last} being the last value of I_g before the step, a relative error of $\frac{leak - I_{last}}{I_{leak}} = 2\%$ is found, which is a reasonable error for an automated estimation of the leakage current. When however comparing the estimated leakage current and I_{last} for higher values of V_G, for example near t = 2000s, we find a much higher relative error of 21%. This is obviously a substantial error , which might explain the high values of n_{doping} that are obtained. The maximum doping density of F8BT can be calculated if the molecular weight of one repeat unit $C_{35}H_{42}N_2S$[11] of the F8BT polymer is known. The molecular mass of one repeat unit $C_{35}H_{42}N_2S$ is M = 0,5 kg/mol. This corresponds to 10^{-24} kg per repeat unit. Assuming the density of the F8Bt in the layer is equal to the water density $\rho = 10^3 \mathrm{kg/m^3}$, we find the number of F8BT repeat units in the channel to be[10] $\frac{V_{channel} \cdot N_a}{V_{cell}} \approx 10^{28}$, with N_a Avogadro’s constant. Here the limit is about one electron per three F8BT units. This gives us a maximum value of $3 \cdot 10^{27}\, m^{-3}$ for the doping density, a value that is broadly exceeded by the calculated values of the doping density in this series. Reason for these flaws in the measured results might be side reactions that happen because of the way the electrolyte is applied. As described in section 3.2Samples the electrolyte is dissolved in acetone. The acetonitrile used for the second F8BT measurement series is produced purer in the sense that it contains less water than the acetone. The manufacturer has used distillation processes in order to make it contain less water. The imperfections of the acetone can lead to side reactions which can subvert our measurements for higher gate voltages.

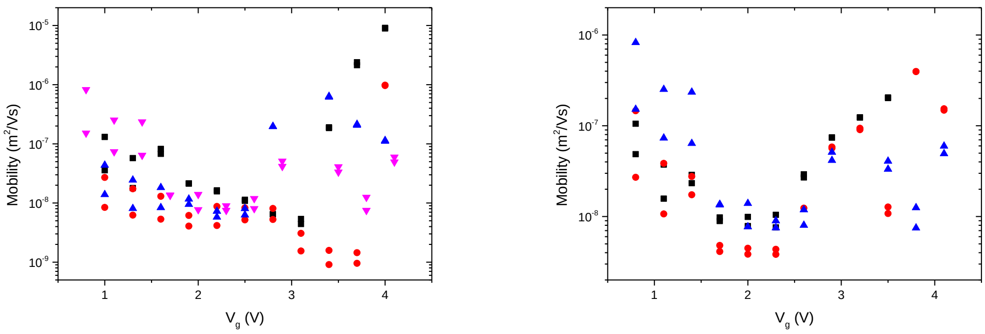

Figure 21 A summary of the mobility calculations of the first seris of F8BT measurements.

The obtained **mobility** μ of charge carriers in the active layer is displayed in **Error! Reference source not found.**. Since the mobility is calculated using equation 3, so $\mu = \frac{\sigma}{e \cdot (n_{doping} + n_{sc})}$,it is highly dependent on the behaviour of the doping density and conductivity. However, as described earlier in this section, the conductivity and the doping density results in this series are quite inaccurate, meaning a high error in the resulting mobility is impossible to get around. Even with the error in the conductivity taken into account, a unexpected shape of the mobility graph is observed for low values of the gate voltage for every sample measurement. In particular, the mobility is descending for increasing gate voltage. A possible explanation for this unexpected behaviour may lie in the calculation of μ, where we do not take into account the initial current density n_{sc} of our active layer. For a higher value of the gate voltage, the doping density is much higher in magnitude compared to n_{sc}, so this estimation does not have a lot of influence on the calculation of the mobility. However, for lower doping density values, the initial charge carrier density starts having a considerable contribution to the calculation. When not taking n_{sc} into account when calculating the mobility, this results in a higher value of the mobility than expected and consequently a decadence of the graph. Apart from this unexpected behaviour we do find that the order of magnitude of the mobility corresponds to the value found in the literature[11].

5.3 F8BT – second series

The devices in this measurement series are also organic electrochemically gated transistors with an active layer consisting of F8BT. These devices contain an electrolyte also based on PEO with KTF, but for this series the solvent used for the electrolyte is acetonitrile. Apart from that, in these experiments the way of measuring is the same as described in the previous sections. The acetonitrile is used because this contains less water, which minimizes the perturbation possibly caused by the occurring side reactions while doping the active layer.

5.2.1 Measurements

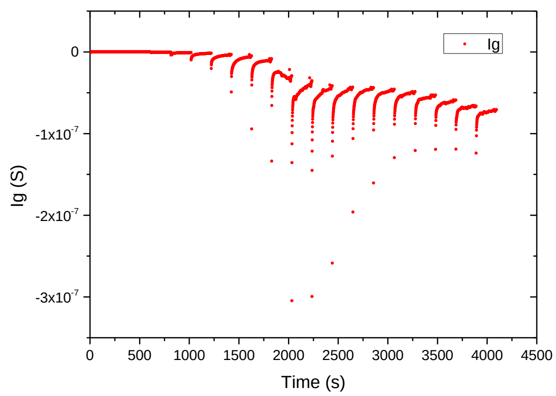

Figure 22 A typical measurement on a sample of the second F8BT series.

Since less perturbation is observed in the gate current plots of these samples for high gate voltages, the relative error in leakage current $\frac{leak - I_{last}}{I_{leak}} = 2\%$ is more or less constant throughout all of the measurements. This 2% uncertainty is due to the sensitivity of the measurement setup. Due to the lower amount of side reactions happening for higher gate voltages, the uncertainty in the estimation of the leakage current for high values is ten times as low as in the previous series.

5.2.2 Results and discussion

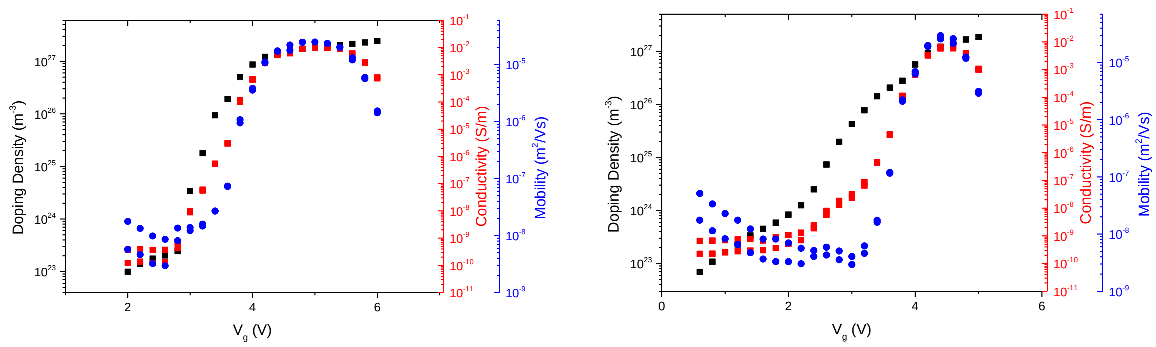

Figure 23 Two typical measurements on samples from the second F8BT series.

For this series the same calculations were used as described in **Error! Reference source not found.**, since however the production of the used samples is adapted to minimize side reactions, we find that the **doping density** behaves as expected for higher values. Due to the lower perturbation in the measurements represented in figure 22, the doping density does not exceed the expected limiting value of $3 \cdot 10^{27}\ \mathrm{m}^{-3}$.

For lower values of V_g¸ the calculated **conductivity** still has the high uncertainty due to the hysteresis in the current measurements. As expected this was independent of the solvent used for the electrolyte. In a next series, it would seem meaningful to find a way to dispose the occurring hysteresis, to minimize the uncertainty in the determination of the conductivity for lower gate voltages. One possible way would be to accompany the high source-drain voltage changes with a sort of settling time. More gradually changing the source-drain voltage would be another approach to prevent hysteresis from occurring. For high values of the gate voltage we find a new behaviour of the conductivity, being that it decays deliberately. This course of the graphs can be explained by applying the theory in

2.5 . The Gaussian shape of the density of states of the used material (F8BT) results in a conductivity that increases at first, due to the Fermi level rising along the exponential tail of the Gaussian shape. After becoming a constant, the Gaussian shape starts decaying exponentially for a higher Fermi level. So when filling up even more states by injecting the material with charge carriers, the conductivity will also decay for a higher Fermi level.

The same behaviour of the **mobility** is observed from these samples at low gate voltages. The reason for this is that also for the mobility the calculations have not changed, so still the n_{sc} is not taken into account. For high values of V_g, to be more specific when the doping density starts to saturate, we find a lower mobility of the charge carriers. This is easily derived from the fact that the conductivity of the material decays while the doping density is near constant. Following $\mu = \frac{\sigma}{e \cdot (n_{doping} + n_{sc})}$ the mobility will simply decay for decreasing conductivity.

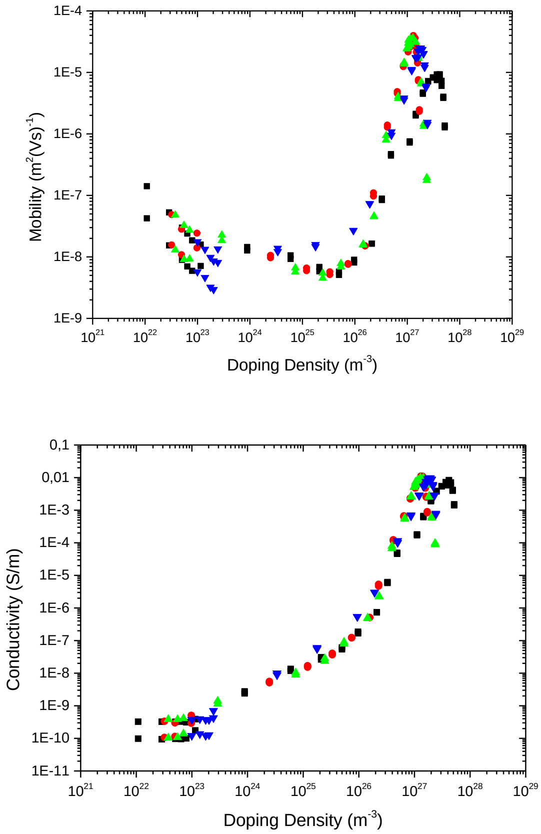

Figure 24 The mobility and the conductivity for four measurements on one sample of the second F8BT series plotted against the doping density.

The above results display the direct effect of controlled doping on the mobility and conductivity of the measured F8BT sample. Measurement *red, blue* and *green* display the exact same behaviour for both the mobility and the conductivity. An increasing doping density enhances both the conductivity and the mobility until a certain maximum is achieved of $\sigma = 0{,}01$ S/m and $\mu = 10^{-5}\mathrm{m}^2/\mathrm{Vs}$. This as opposed to the initial values of respectively $\sigma = 10^{-10}$ S/m and $\mu = 10^{-8}\mathrm{m}^2/\mathrm{Vs}$, which shows an increase in the order of magnitude for the conductivity of 10^5 and for the mobility of 10^3. Further enhancing the doping density results in a decrease in mobility as well as conductivity, as expected to be a result of the Gaussian shape of the density of states. Raising the Fermi level beyond the maximum of the Gaussian DOS shape by injecting carriers into the material will result in less delocalised carriers, hence a lower conductivity and a lower mobility as described earlier in this section.

6 Conclusion

The aim of this experiment was to optimize the power factor $S^2\sigma$ and thus ZT using controlled doping.

In this report experiments are described to measure the Seebeck coefficient of a semiconducting polymer. This experiment has been performed on PEDOT:PSS PH1000 yielding Seebeck coefficients in the range of $S = 10^{-5}$ V/K.

Using organic electrochemically gated transistor devices the effects of doping on the electrical properties of several organic semiconductors have been studied. In summary, we have measured the doping density, conductivity and mobility of these devices, containing the organic semiconductors Super-Yellow PPV and F8BT. The solvent used for the electrolyte has been altered between two measurement series, resulting in the uncertainty in doping density measurements decreasing by a factor ten in some cases. Because of this increase of quality of our measurements we were able to determine the direct effect of controlled doping on the mobility and conductivity of a F8BT sample.

There is room for more optimisation in this experiment, not only by adjusting the used calculations, but also by making alterations to the used source-drain sweep measurements.

Since the described experiments have not been combined into one experiment to optimize the power factor $S^2\sigma$ using controlled doping, these experiments might serve a preliminary role for an experiment to optimize the power factor and thus the figure of merit using controlled doping.

7 Outlook

The aim of this experiment was to optimize the power factor $S^2\sigma$ and thus ZT using controlled doping. Using organic electrochemically gated transistor devices the effects of doping on the electrical properties of several organic semiconductors have been studied. However, the effect of doping the active material on the Seebeck coefficient has been left open for future research.

The experiment shown in this report can be enhanced in several ways. First method is taking into account hysteresis when measuring current. Giving a high bias voltage difference a higher settling time for example would prevent the high uncertainty in conductivity measurements in the low doping density region. For these lower values of the doping density, also an unexpected behaviour of the mobility is observed. This behaviour could be further examined by taking into account the initial carrier density present in the used device. These efforts would be effective in minimizing perturbations on the measured electrical properties of the used materials.

The next step after this experiment would be to measure the Seebeck coefficient of the organic semiconductors, while applying controlled doping using organic electrochemically gated transistor devices. The results of this experiment could be used to optimize the figure of merit *ZT.*

10 Sources

[1] Yi Li, Daniel Lu, C. P. Wong, Electrical Conductive Adhesives with Nanotechnologies, **2010**

[2] Max Scheepers, Martijn Kemerink, Stephan van Reenen, Seebeck Coefficient and Electrical Conductivity Measurements on Poly(3,4-ethylenedioxythiophene)poly(styrenesulfonate) Films Treated with Sulfuric Acid, *bachelor thesis,* **2013**

[3] W. Chr. Germs, Moving charged particles in fluctuating and disordered energy landscapes, *thesis,* **2013,** 66, 70, 81

[4] David Nemir, Jan Beck, On the Significance of the Thermoelectric Figure of Merit Z, *Journal of ELECTRONICAL MATERIALS Vol.29 No.9,* **2010**

[5] A. F. Ioffe, Semiconductor thermoelements, and Thermoelectric cooling, **1957**

[6 Stephan van Reenen, Martijn Kemerink, Correcting for contact geometry in Seebeck coefficient measurements of thin film devices, *Organic Electronics 15*, **2014**

[7] Seung Hwan Lee, Hongkwan Park, Soyeon Kim, Woohyun Son, In Woo Cheong and Jung Hyun Kim, Transparent and flexible organic semiconductor nanofilms with enhanced thermoelectric efficiency, *J. Mater. Chem. A,* **2014**

[8] Hikmat Najafov, Ivan Biaggio, Ta-Ko Chuang, and Miltiadis K. Hatalis, Exciton dissociation by a static electric field followed by nanoscale charge transport in PPV polymer films, *Phys. Rev. B 73,* **2006**

[9] S.R. Tsenga, Y.S. Chena, H.F. Menga,∗, H.C. Lai b, C.H. Yehb, S.F. Horng b, H.H. Liao b, C.S. Hsuc, Electron transport and electroluminescent efficiency of conjugated polymers, *Synthetic Metals 159,* **2009**

[10] Hidekazu Shimotani, Gildas Diguet, Yoshihiro Iwasa, Direct comparison of field-effect and electrochemical doping in regioregular poly(3-hexylthiophene), *Applied Physics Letters 86,* **2005**

[11] Sigma-Aldrich, Product Specification: product number 698687, http://www.sigmaaldrich.com/Graphics/COfAInfo/SigmaSAPQM/SPEC/69/698687/698687-BULK ALDRICH .pdf , **09-2014**